Leading-Edge and Ultra-Thin 3D Glass-Polymer 5G Modules with Seamless Antenna-to-Transceiver Signal Transmissions

Atom O. Watanabe, Tong-Hong Lin,
P. Markondeya Raj,Venky Sundaram, Manos M. Tentzeris, and Rao R. Tummala
3D Systems Packaging Research Center
Georgia Institute of Technology
Atlanta, GA USA
email: atom@gatech.edu

Tomonori Ogawa
Asahi Glass Company
Tokyo, Japan
email: togawa@agcem.com

***Abstract*— This paper demonstrates seamless antenna-to-transceiver signal transitions on panel-scale processed ultra-thin glass-based 5G modules with impedance-matched transmission lines and microvias with high-precision low-loss re-distribution layer design and fabrication, for high-speed 5G communication standards at the 28 GHz band. In order to demonstrate the benefits of glass for 5G communications, various types of transmission lines and high-gain and high-bandwidth package-integrated antennas were modeled and designed on ultra-thin glass substrates with low-loss dielectric thin-films, for highest bandwidth and efficiency in the mm-wave bands. The simulated results for insertion losses of transmission lines (i.e., microstrip lines and striplines) and microvia transitions are correlated with the measured values on the thin glass substrates. In addition to the low-loss signal transitions from chip to antenna, package-integrated Yagi-Uda antennas are modeled and designed, resulting in a realized gain of higher than 4 dBi/element with a bandwidth higher than 20%. The mm-wave electrical performance of glass substrates was benchmarked with existing 5G candidates such as organic laminate substrates and fanout wafer level packaging. Along with the reduction in the overall package foot-print, reduction in link-budget losses is shown to be feasible with the proposed 3D glass packages.**

Index Terms*— *5G communications, Glass packaging, Low loss interconnects, Microvia, Transmission lines, Antenna in package, Yagi-Uda antenna

I. INTRODUCTION

It is expected that the fifth-generation (5G) mobile network services will, by 2020, provide customers with 40X higher communication speed than the recent networks. This evolution will lead to an increase in the amount of global data traffic with 8X between 2015 and 2020 and 80X between 2020 and 2025. Such ultra-high speed communications with low-latency ($<$ 1 ms) will enable massive-data technologies such as highly-reliable self-driving automotive, upgraded medical services, ubiquitous network, Internet of Things (IoT), high-definition video streaming at a resolution of 4K and higher [1]. With such trends, IC packaging technologies for high frequencies ranging from 5 GHz through 74 GHz, which enable such high-speed communications, are recently gaining more attention. From the standpoint of standards, regulations, and solutions for consumer daily use, recent focus is on frequency bands around 28, 39, 60, and 73 GHz [2], [3].

In order to meet the performance requirements at these bands, novel packaging technology in the mm-wave frequency range that addresses fundamental mm-wave technical challenges such as low-loss and ultra-broadband interconnects, high routing density, thin packaging substrates, high-performance integrated passive devices (IPDs), and form-factor reduction is required. In addition, improved electromagnetic interference shielding performance along with a strong focus on cost reduction will play a significant role for mm-wave front-end modules with package-integrated-antenna structures used in the 5G mobile era [1], [4]. One of the most significant factors is the low-loss link budget and short interconnects from chip to antenna to transmit and receive modulated signals efficiently.

State-of-the-art packages for high-frequency communications employ ceramics, organic laminates, and silicon substrates, and fan-out packages with epoxy molding compounds. Ceramic substrates are preferred because of their low-loss properties, low moisture absorption, and stable properties in high frequency ranges [5]. The limitations of cost and form-factor reduction of ceramic substrates lead to the popularity of organic substrates. Liu *et. al.* demonstrated fully-integrated antenna-in-packages (AiP) in organic substrates in the W band using a fully-operational compact transceiver package with 64 dual-polarized antennas [2], [6]. Moreover, Saily *et. al.* has explored ultra-low-loss organics based on liquid-crystal polymers (LCP) and showed antenna gains as high as 23 dBi and an operational bandwidth of 2 GHz [7], [8]. In recent years, the evolution of embedded fanout packages technologies such as fan-out wafer-level packaging (FOWLP) opened the new era in pack-

2377-5726/18/$31.00 ©2018 IEEE
DOI 10.1109/ECTC.2018.00304

aging, enhancing performances, form factor, and package reliability. This technology enabled elimination of the use of wire-bonding thereby reducing the total link budget and increasing the foot-print for high-pin count dies. Moreover, this technology enable double-sided multiple re-distribution layers (RDL) to fan-out input/output signals with through-mold vias, leading to vertical interconnections [9], [10], [11].

State-of-the-art packaging technologies lead to several fundamental barriers and challenges to achieve high precision and tolerance that are required for mm-wave components in the dimension of a few microns [12], [13], [14]. As an ideal evolution to address these challenges, glass-based packaging technology has been recently gaining attention due to its ability to form fine-pitch line and spaces [15] and through-vias [16], robustness against high temperature and humidity, dimensional stability [17], matched coefficient of thermal expansion (CTE) with silicon dies, and large-area low-cost panel-scale processability [18].

This paper discusses the design and demonstration of high-bandwidth fully-integrated AiP with low-loss link budget from chip to antenna using glass-packaging technology. Low-loss dielectric thin-films on 100 μm glass core are utilized as the glass substrates with double-side routing and interconnect layers, as shown in Figure 1. Section II focuses on modeling and design of low-loss chip-to-antenna interconnects such as transmission lines and microvias, and Yagi-Uda antennas in polymer-laminated glass substrates. Section III discusses the fabrication of the test vehicles to realize those designs. Finally, Section IV shows the electrical characterization and analyses of the fabricated test vehicles while the conclusions are compiled in Section V.

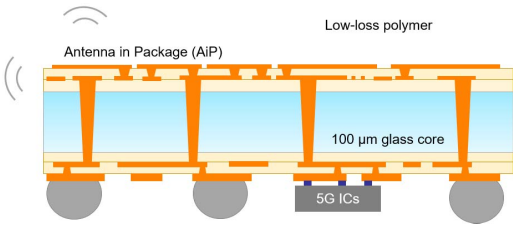

Fig. 1. Cross-section image of 3D glass-polymer 5G modules.

II. MODELING AND DESIGN OF LOW-LOSS INTERCONNECTS AND PACKAGE-INTEGRATED ANTENNAS

The objective of this task is to design various types of low-loss transmission lines with microvia transitions in low-loss dielectric polymer thin-films, and package-integrated Yagi-Uda antenna structures. For these designs, EN-A1 100-μm glass core substrates from Asahi Glass and GL102 dielectric thin-films are selected because of their low dielectric properties and superior handing.

A. Low-loss transmission lines with microvia transitions

In order to demonstrate superior performance of routing and interconnect layers on thin glass substrates with low-loss dielectric thin-films, six-metal-layer test vehicles with interconnects such as transmission lines and microvia transitions were designed. Transmission-line structures include microstrip lines (Figure 2 (a)) and striplines embedded in low-loss dielectric thin-films (Figure 2 (b)). In the designs, 50-Ω microstrip-line and stiripline widths were determined to be 65.6 μm and 6.6 μm from the standing point of impedance matching. Moreover, in order to obtain losses from microvias between the interconnect layers, microvias with a diameter of 40 μm are designed for transitions from a microstrip line to a stripline or vice versa, as shown in Figure 2 (c).

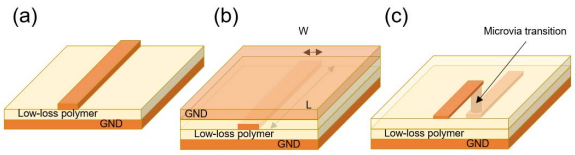

Fig. 2. 3D view of (a) microstrip lines ,(b) striplines, and (c) microvia transitions on low-loss dielectric thin-films.

Utilizing these interconnect designs, 3D full-wave EM simulations through the HFSS software were performed. Simulations results are illustrated in Figure 3. The results indicate that transmission lines provide an average loss of 0.100 dB/mm and that microvias provide an averaged loss of 0.023 dB/microvia both at 28 GHz, calculated from the coupons with microvia transitions, after de-embedding the transmission-line losses. These numbers lead to low-loss link budget from chip to package-integrated antenna that is discussed in Section II B.

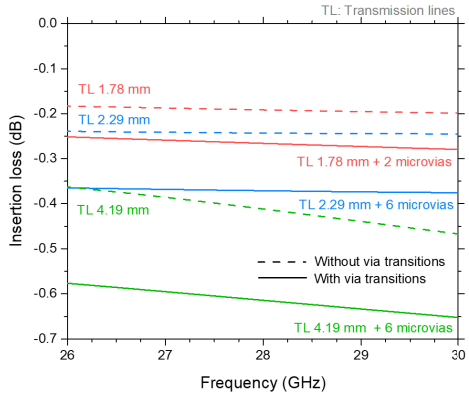

Fig. 3. Simulation results of transmission-line and microvia losses.

B. Package-integrated Yagi-Uda antennas

This section briefly discusses the designs of package-integrated Yagi-Uda antennas on low-loss dielectric thin-films laminated on glass core substrates. Yagi-Uda antennas are employed to enable miniaturized structures and to obtain high gain with high bandwidths and good angle coverage [19]. As illustrated in Figure 4, the structure, first, requires a quarter-wave transformer to match the impedances from

transmission lines (50 Ω) to a two-port divider (25 Ω each). The divider is connected to a balun phase shifter that generates 180° phase difference between the coupled microstrip lines at the operating frequency, enabling the correct excitation towards the driven element. When designing the balun phase shifter, a standard method, the angled miter, was employed to minimize the characteristic-impedance changes while moving through the bend, which degrade the overall antenna performance. A co-planar stripline was introduced to separate the driven element from the reference plane so that the reference plane acts as a reflector. In this antenna topology, only one director in the direction of desired radiation was added so as to obtain a certain level of realized gain and good coverage with high bandwidths higher than 20%. The simulation results of the designed antenna are shown in Section IV.

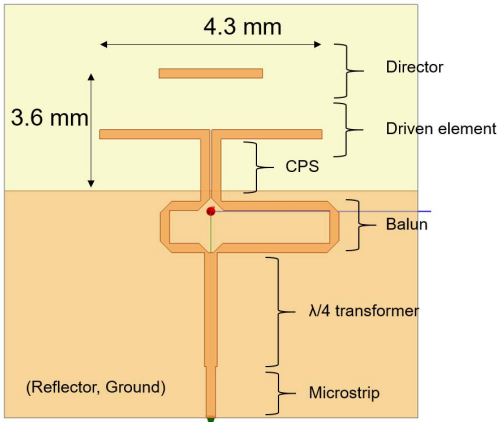

Fig. 4. Yagi-Uda antenna configuration designed on low-loss polymer thin-films laminated glass.

III. FABRICATION OF TRANSMISSION LINES AND MICROVIA TRANSITIONS IN LOW-LOSS DIELECTRIC THIN-FILMS

This section discusses the fabrication of the designed signal-traces on low-loss dielectric thin-films that are laminated onto glass core substrates. The impact of fabrication on electrical performance is also discussed.

In order to fabricate the designed test vehicles with high precision and tolerance, semi-additive patterning (SAP) process is employed. When processed on glass substrates, SAP enables very fine-feature line and space fabrication because of their dimensional stability and surface planarity. One of the fabricated test vehicles is depicted in Figure 5, which includes 50-Ω microstrip lines (Figure 5 (b)) and microstrip-stripline transitions with microvias (Figure 5 (c)). Cross sectioning for both a side view and a front view was performed to verify the physical dimensions of striplines that have the smallest feature size (6.6 μm) in these test vehicles. The cross-sectioned images are shown in Figures 6 and 7.

The widths of the fabricated transmission lines were measured through optical microscopy and the measurement

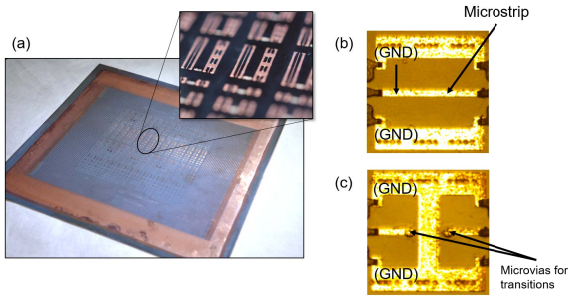

Fig. 5. Fabricated glass panel with low-loss interconnects, with the inset of a magnified image.

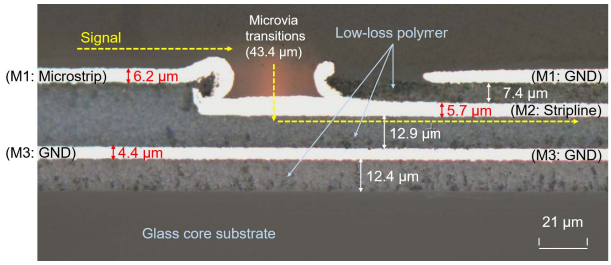

Fig. 6. Side view of the cross-sectioned transmission liens and microvia transitions designed for the 28 GHz band.

results are listed in Table I. The measured widths of more than twenty coupons for each test vehicle are averaged to remove the dependence on the selected locations across a panel.

While precision of 7-9% with 6-μm striplines was observed, high precision of less than 2% was achieved amongst 65.6-μm microstrip lines. For both the transmission-line structures, the SAP process enabled high precision and tolerance of less than 1.34 μm. Although state-of-the-art high-frequency modules do not entail signal traces or input/output at such small dimensions of a few microns, the next-generation 5G modules are expected to require high precision and control of such low-loss interconnects to enable high-performance IPDs, high routing density, etc.

The thickness of low-loss dielectric thin-films was 12.4–13.0 μm below M2 and M3, while the target is 15 μm, as depicted in Figure 6. Similarly, the dielectric film thickness between M1 and M2 was averaged as 7.3 μm, while the target was 7 μm in the designs. Copper thicknesses for RDLs and the ground plane were 5.7–6.5 μm and 4.4 μm, respectively. Although the thickness of the ground plane does not significantly affect the electrical performance, the deviation of RDL thicknesses may change characteristic impedance and, thus, impedance mismatch that brings about undesired signal reflections and EM radiation that degrades the performance of adjacent components.

IV. ELECTRICAL CHARACTERIZATION OF INTERCONNECTS AND ANTENNAS

Electrical characterization of the fabricated low-loss interconnects with transmission lines and microvias were per-

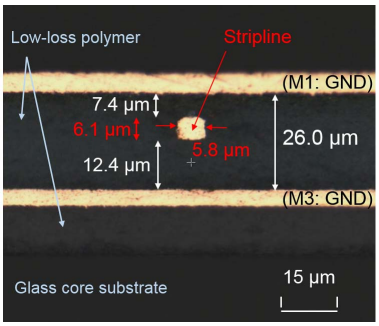

Fig. 7. Front view of the cross-sectioned stripline designed for the 28 GHz band.

TABLE I

RDL PRECISION FABRICATED IN LOW-LOSS POLYMER LAMINATED ON GLASS SUBSTRATES

	TV#1	TV#2	TV#1	TV#2
	Microstrip		Stripline	
Target	65.6 μm		6.6 μm	
Measurements	65.13 μm	67.11 μm	6.62 μm	5.60 μm
Variance	0.95 μm	1.34 μm	0.52 μm	0.60 μm
Precision	1.46%	1.99%	7.88%	9.09%

formed in the frequency domain in order to compare the measurement results with simulation results. The data obtained from the measurements were also analyzed. Furthermore, the performance of the package-integrated Yagi-Uda antenna is shown in this section.

A. Measurement results of insertion losses in low-loss interconnects

In order to verify the simulation results, frequency responses of the designed microstrip lines, striplines, microvias, and the combination of them are measured through a two-port vector network analyzer in the frequency rage of 26–30 GHz. The results, illustrated in Figure 8, show the insertion losses only by transmission lines (Figure 8 (a)) and by transmission lines with microvia transitions (Figure 8 (b)). Although the overall responses from measurements are consistent with those from simulations, ripples were observed in both of the measurements. This phenomenon is attributed to a certain level of impedance mismatch from 50 Ω that causes wave reflections within the device under test. Impedance mismatch is not caused simply by a change in transmission-line width but also by the deviation of dielectric thickness, conductor thickness, conductor surface roughness, as observed in Section III, and tapered angle of signal traces as observed in the stripline shown in Figure 7.

From the frequency responses obtained from each test structure, the losses from transmission lines and microvia transitions are de-embedded, as shown in Figure 9. Based on the results, insertion loss per unit length (mm) for transmission lines and that per microvia are calculated using the linear regression method. Transmission-line losses were measured as 0.103 dB/mm, which is 3% higher than that from the simulations. Although this is mainly caused by the

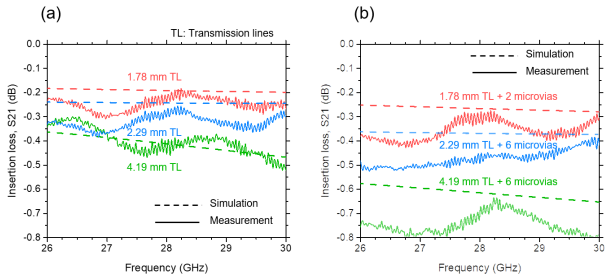

Fig. 8. Frequency responses of signal interconnects in RDL (a) without and (b) with microvia transitions.

slight impedance mismatch discussed above, this range of deviation does not significantly degrade the performance of a system.

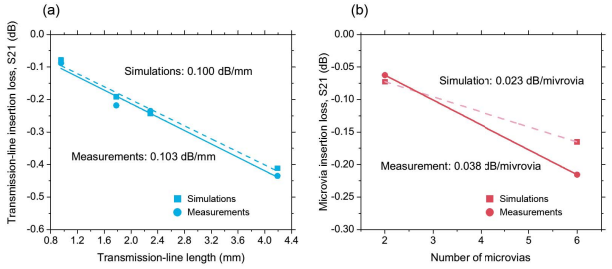

Fig. 9. Insertion losses of (a) transmission lines and (b) microvias in RDL at 28 GHz.

In contrast, the averaged microvia loss was 0.038 dB/microvia, which is 1.65 times higher than that obtained from simulations. In addition to several factors such as copper roughness and deviation of the thicknesses of copper deposited in microvias, the most significant factor that caused this deviation is the topology difference between simulations and the actual fabricated microvias. In simulations, fully-filled vias are assumed for modeling simplicity requiring less number of mesh in the finite-element method used in HFSS. Actual fabricated microvias, however, are based conformal vias, as inspected in Figure 6. Conformal-via models lead to high accuracy and, therefore, good consistency between simulations and measurements, but such modeling entails more number of mesh and a complicated setup in simulations. To verify the difference in losses between fully-filled vias and conformal ones, EM simulations for single via were performed through HFSS as shown in Figure 9. The frequency responses show that conformal vias will cause higher loss because of higher resistance and parasitic inductance. Since thousands of conformal vias are generally modeled in module designs, it is important to assume that the actual measurements will generate around 10–50% higher losses than that of the simulated losses. Another solution to achieve low insertion loss and good model-to-hardware correlation is the fabrication of fully-filled vias that feature superior signal and power integrity, higher reliability, and tolerance to high

temperature and humidity.

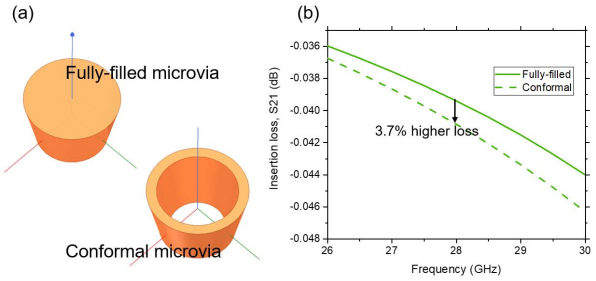

Fig. 10. Configurations of fully-filled and conformal microvias, and their simulated insertion losses.

B. *Package-integrated Yagi-Uda antenna*

This section discusses HFSS electrical simulations of the designed package-integrated Yagi-Uda antenna structure. The preliminary Yagi-Uda antenna without feedlines was designed such that return loss, S_{11}, shows the zero at the vicinity of 28 GHz. This structure provides a bandwidth of 6.4%, which does not satisfy the target bandwidth of 20%. Besides, the structure offered a realized gain of 6.9 dBi, which is too high for handset wireless applications. In order to achieve higher bandwidth and lower gain with a good coverage, the "splitting of zeros" technique was employed for designing broadband Yagi-Uda antenna. The zeros that are generated by the feedline and the radiator are designed at separate frequencies so that there would be two zeros in the return loss, leading to higher operational bandwidths.

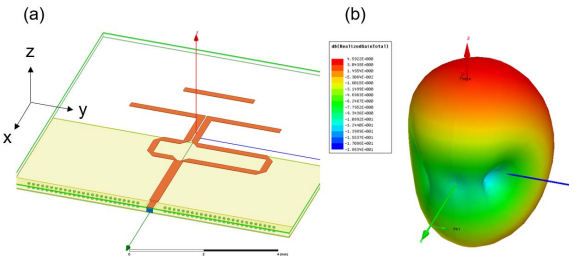

Fig. 11. Designed Yagi-Uda antenna topology with its radiation pattern at the center frequency, 28 GHz.

The optimized Yagi-Uda antenna topology and its radiation pattern are depicted in Figure 11. In addition to the 3D configuration, the resultant frequency responses are illustrated in Figure 12 (a), showing the two zeros with a bandwidth of 23.4% led by the radiator and the feedline. Figure 12 (b) shows the realized gain in the x-z plane and x-y plane with a wide range of coverage. This antenna topology will be useful for various types of applications because of the high bandwidth with good coverage.

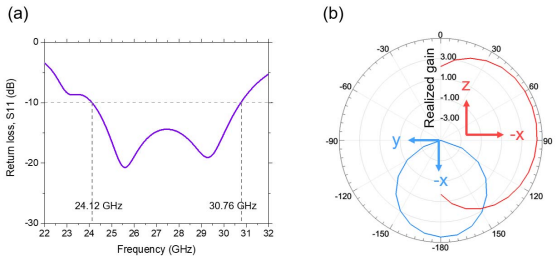

Fig. 12. (a) Return loss of the antenna with the feedline (b) radiation patterns in the x-z and x-y planes.

V. CONCLUSIONS

This paper demonstrates seamless antenna-to-transceiver signal transitions on panel-scale processed ultra-thin glass based 5G modules with impedance-matched transmission lines and microvias with high-precision low-loss routing and interconnect layers, for high-speed 5G communication standards at the 28 GHz band. Various topologies of transmission lines, interconnects, and a high-gain and high-bandwidth package-integrated Yagi-Uda antenna were modeled and designed on ultra-thin glass substrates with low-loss dielectric thin-films, for highest bandwidth and efficiency in the mm-wave bands. The simulated results for insertion losses of transmission lines (i.e., microstrip lines and striplines) and microvia transitions were correlated with the measured values on glass substrates with low-loss dielectric thin-films. Transmission lines in the build-up routing layers showed an averaged insertion loss of 0.103 dB/mm, while that on microvia was observed to be 0.038 dB/microvia. Along with the reduction in the overall package foot-print, about 3X reduction in link-budget losses compared to fanout wafer level packaging is shown to be feasible with the proposed 3D glass packages. In addition to the low-loss signal transitions from chip to antenna, a package-integrated Yagi-Uda antenna was modeled and optimized, resulting in a realized gain of 4.6 dBi/element with a bandwidth of 23.4%. These low-loss interconnects on build-up dielectric thin-films on glass and the package-integrated Yagi-Uda antenna will enable high-performance 5G antenna modules.

ACKNOWLEDGMENT

The authors wish to acknowledge engineers from Qualcomm for their supportive advice on designs and Hiroyuki Matsuura from NGK Spark Plug Co. for helping with the fabrication of test vehicles. They also would like to thank the industry sponsors of the consortia program at Georgia-Tech Packaging Research Center (GT-PRC) for their technical guidance and support.

REFERENCES

[1] T. Nishio, "Electronic packaging gears up for 5g mobile race," in *Electronics Packaging (ICEP), 2017 International Conference on*. IEEE, 2017, pp. 328–332.

[2] D. Liu, X. Gu, C. W. Baks, and A. Valdes-Garcia, "Antenna-in-package design considerations for ka-band 5g communication applications," *IEEE Transactions on Antennas and Propagation*, vol. 65, no. 12, pp. 6372–6379, 2017.

[3] D. Liu and Y. Zhang, "Integration of array antennas in chip package for 60-ghz radios," *Proceedings of the IEEE*, vol. 100, no. 7, pp. 2364–2371, 2012.

[4] A. O. Watanabe, S. Jeong, S. Kim, Y. Kim, J. Min, D. Wong, M. R. Pulugurtha, R. Mullapudi, J. Kim, and R. R. Tummala, "Highly-effective integrated emi shields with graphene and nanomagnetic multilayered composites," in *Electronic Components and Technology Conference (ECTC), 2016 IEEE 66th*. IEEE, 2016, pp. 206–210.

[5] Y. P. Zhang and D. Liu, "Antenna-on-chip and antenna-in-package solutions to highly integrated millimeter-wave devices for wireless communications," *IEEE Transactions on Antennas and Propagation*, vol. 57, no. 10, pp. 2830–2841, 2009.

[6] X. Gu, D. Liu, C. Baks, A. Valdes-Garcia, B. Parker, M. R. Islam, A. Natarajan, and S. K. Reynolds, "A compact 4-chip package with 64 embedded dual-polarization antennas for w-band phased-array transceivers," in *Electronic Components and Technology Conference (ECTC), 2014 IEEE 64th*. IEEE, 2014, pp. 1272–1277.

[7] C.-Y. Ho, M.-F. Jhong, P.-C. Pan, C.-Y. Huang, C.-C. Wang, and C.-Y. Ting, "Integrated antenna-in-package on low-cost organic substrate for millimeter-wave wireless communication applications," in *Electronic Components and Technology Conference (ECTC), 2017 IEEE 67th*. IEEE, 2017, pp. 242–247.

[8] J. Säily, M. Pokornỳ, M. Kaunisto, A. Lamminen, J. Aurinsalo, and Z. Raida, "Millimetre-wave beam-switching rotman lens antenna designs on multi-layered lcp substrates," in *Antennas and Propagation (EuCAP), 2016 10th European Conference on*. IEEE, 2016, pp. 1–5.

[9] C.-H. Tsai, J.-S. Hsieh, M. Liu, E.-H. Yeh, H.-H. Chen, C.-W. Hsiao, C.-S. Chen, C.-S. Liu, M.-J. Lii, C.-T. Wang *et al.*, "Array antenna integrated fan-out wafer level packaging (info-wlp) for millimeter wave system applications," in *Electron Devices Meeting (IEDM), 2013 IEEE International*. IEEE, 2013, pp. 25–1.

[10] C.-W. Hsu, C.-H. Tsai, J.-S. Hsieh, K.-C. Yee, C.-T. Wang, and D. Yu, "High performance chip-partitioned millimeter wave passive devices on smooth and fine pitch info rdl," in *Electronic Components and Technology Conference (ECTC), 2017 IEEE 67th*. IEEE, 2017, pp. 254–259.

[11] J. Bock and R. Lachner, "Sige bicmos and ewlb packaging technologies for automotive radar solutions," in *Microwaves for Intelligent Mobility (ICMIM), 2015 IEEE MTT-S International Conference on*. IEEE, 2015, pp. 1–4.

[12] V. Sundaram, B. Deprospo, N. Gezgin, A. Watanabe, P. M. Raj, F. Liu, W. Puckett, S. Graham, R. Tummala, K. Byers *et al.*, "Integrated copper heat slugs and emi shields in panel laminate (lfo) and glass fanout (gfo) packages for high power rf ics," in *Electronic Components and Technology Conference (ECTC), 2017 IEEE 67th*. IEEE, 2017, pp. 300–305.

[13] A. O. Watanabe, M. Ali, B. Tehrani, J. Hester, H. Matsuura, T. Ogawa, P. M. Raj, V. Sundaram, M. M. Tentzeris, and R. R. Tummala, "First demonstration of 28 ghz and 39 ghz transmission lines and antennas on glass substrates for 5g modules," in *Electronic Components and Technology Conference (ECTC), 2017 IEEE 67th*. IEEE, 2017, pp. 236–241.

[14] T. H. Lin, P. M. Raj, A. Watanabe, V. Sundaram, R. Tummala, and M. M. Tentzeris, "Nanostructured miniaturized artificial magnetic conductors (amc) for high-performance antennas in 5g, iot, and smart skin applications," in *2017 IEEE 17th International Conference on Nanotechnology (IEEE-NANO)*, July 2017, pp. 911–915.

[15] F. Liu, C. Nair, A. Kubo, T. Ando, H. Lu, R. Zhang, H. Chen, K. S. Lee, V. Sundaram, and R. R. Tummala, "Via-in-trench: A revolutionary panel-based package rdl configuration capable of 200-450 io/mm/layer, an innovation for more-than-moore system integration," in *Electronic Components and Technology Conference (ECTC), 2017 IEEE 67th*. IEEE, 2017, pp. 2097–2103.

[16] S. Viswanathan, T. Ogawa, K. Demir, T. B. Huang, P. M. Raj, F. Liu, V. Sundaram, and R. Tummala, "High frequency electrical performance and thermo-mechanical reliability of fine-pitch, copper-metallized through-package-vias (tpvs) in ultra-thin glass interposers," in *Electronic Components and Technology Conference (ECTC), 2017 IEEE 67th*. IEEE, 2017, pp. 1510–1516.

[17] S. McCann, V. Smet, V. Sundaram, R. R. Tummala, and S. K. Sitaraman, "Experimental and theoretical assessment of thin glass substrate for low warpage," *IEEE Transactions on Components, Packaging and Manufacturing Technology*, vol. 7, no. 2, pp. 178–185, 2017.

[18] C. Buch, D. Struk, K. J. Wolter, P. J. Hesketh, V. Sundaram, R. Tummala, C. Shearer, J. Haley, M. Findlay, and M. Papageorge, "Design and demonstration of highly miniaturized, low cost panel level glass package for mems sensors," in *2017 IEEE 67th Electronic Components and Technology Conference (ECTC)*, May 2017, pp. 1088–1097.

[19] H. Karbalaee, M. R. Salehifar, and S. Soleimany, "Designing yagi-uda antenna fed by microstrip line and simulated by hfss," in *Application of Information and Communication Technologies (AICT), 2012 6th International Conference on*. IEEE, 2012, pp. 1–5.